Published in final edited form as:
J Med Chem. 2011 April 28; 54(8): 2687–2700. doi:10.1021/jm101487v.

Synthesis and Evaluation of Radioligands for Imaging Brain Nociceptin/Orphanin FQ Peptide (NOP) Receptors with Positron Emission Tomography

Victor W. Pike[a,*], **Karen S. Rash**[b], **Zhaogen Chen**[b], **Concepción Pedregal**[c], **Michael A. Statnick**[b], **Yasuyuki Kimura**[a], **Jinsoo Hong**[a], **Sami S. Zoghbi**[a], **Masahiro Fujita**[a], **Miguel A. Toledo**[c], **Nuria Diaz**[c], **Susan L. Gackenheimer**[b], **Johannes T. Tauscher**[b], **Vanessa N. Barth**[b], and **Robert B. Innis**[a]

[a]Molecular Imaging Branch, National Institute of Mental Health, National Institutes of Health, Building 10, Rm. B3 C346A, 10 Center Drive, Bethesda, MD 20892, USA

[b]Eli Lilly & Co., Lilly Research Laboratories, Indianapolis, IN 46285, USA

[c]Lilly S.A., Avda. de la Industria 30, 28108-Alcobendas, Madrid, Spain

Abstract

Positron emission tomography (PET) coupled to an effective radioligand could provide an important tool for understanding possible links between neuropsychiatric disorders and brain NOP (nociceptin/orphanin FQ peptide) receptors. We sought to develop such a PET radioligand. High-affinity NOP ligands were synthesized based on a 3-(2'-fluoro-4',5'-dihydrospiro[piperidine-4,7'-thieno[2,3-*c*]pyran]-1-yl)-2(2-halobenzyl)-*N*-alkylpropanamide scaffold and from experimental screens in rats, with ex vivo LC-MS/MS measures, three ligands were identified for labeling with carbon-11 and evaluation with PET in monkey. Each ligand was labeled by ^{11}C-methylation of an *N*-desmethyl precursor and studied in monkey under baseline and NOP receptor-preblock conditions. The three radioligands, [^{11}C](***S***)-**10a–c**, gave similar results. Baseline scans showed high entry of radioactivity into brain to give a distribution reflecting that expected for NOP receptors. Pre-block experiments showed high early peak levels of brain radioactivity which rapidly declined to a much lower level than seen in baseline scans, thereby indicating a high level of receptor-specific binding in baseline experiments. Overall, [^{11}C](***S***)-**10c** showed the most favorable receptor-specific signal and kinetics and is now selected for evaluation in human subjects.

Keywords

NFSI; NOP receptor; PET; Radioligand; Carbon-11; Imaging

Introduction

Nociceptin, also known as orphanin FQ, is the most recently discovered peptide member of the endogenous opioid family.[1,2] Nociceptin acts on specific G-protein coupled receptors that are linked to the cAMP cascade, and to voltage-gated Ca^{2+} and K^+ channels.[3] These

*Author for correspondence: Tel: 301 594 5986. Fax: 301 480 5112. pikev@mail.nih.gov.

Supporting Information: X-ray analysis of (***S***)-**9c and (*R*)-9a**. Supplementary PET scans of [^{11}C]**(*S*)-10c and** [^{11}C]**(*R*)-9a**. HPLC of separation of [^{11}C]-**(*S*)-10c**. HPLC analyses of radioligands [^{11}C](***S***)-**10a–c**.

receptors were formerly known as ORL-1 (opioid receptor-like receptor-1) and are now called NOP (nociceptin opioid peptide) receptors. They are present in various organs including brain and have roles in many normal physiological responses, such as cognition, locomotion, and neuroendocrine control.[3] Additionally, many neuropsychiatric disorders are possibly linked to the NOP receptor, including pain, anxiety, depression, anorexia, obesity and drug abuse.[4,5] Accordingly, the brain NOP receptor is a target not only for biomedical investigation but also for drug therapies.[4]

Positron emission tomography (PET)[6], in tandem with selective radioactive probes (radioligands), is a molecular imaging technique with a unique capability for investigating the living human brain and in particular for investigating specific proteins as possible players in pathophysiology[7] or as targets for therapeutic interventions[8]. Effective PET radioligands now exist for a wide range of targets, selected from among brain enzymes, transporters, plaque, ion channels, and neurotransmitter receptors.[9] Even so, many specific molecular targets of potential interest, including the NOP receptor, still lack a specific radioligand for investigation with PET. PET coupled to an effective NOP receptor radioligand could be an important tool for furthering the understanding of neuropsychiatric disorders in which NOP receptors are implicated, and also for the development of new drugs that may target NOP receptors in the treatment of such disorders. We therefore sought to develop a radioligand for imaging brain NOP receptors with PET.

Effective PET radioligands for imaging in brain must display an array of favorable attributes, including amenability to labeling with a short-lived positron-emitter such as carbon-11 ($t_{1/2}$ = 20.4 min) or fluorine-18 ($t_{1/2}$ = 109.7 min), ability to cross the blood-brain barrier, high affinity and selectivity for binding to the target protein, relatively low non-specific binding, and absence of troublesome brain-penetrant radiometabolites.[10,11,12,13] The difficult challenge of meeting such a combination of requirements in any proposed PET radioligand is a major reason for the current prevalence of non-imageable protein targets. A further important consideration is that the target protein should be present in adequate concentration for potential imaging. As a guideline the product of receptor density (B_{max}, nM) and ligand affinity ($1/K_D$, nM^{-1}) should exceed a value of 5 in target-rich regions of brain.

The distribution of NOP receptors in rat brain has been studied by autoradiography.[14,15,16,17] These studies show a widespread distribution of NOP receptors with, for example, relatively high levels in cortex, hypothalamus and amygdala and low level in striatum. The density of NOP receptors in rat brain membranes was estimated at 237 fmol/mg protein (roughly equating to 24 nM in whole brain).[17] Data on the distribution and density of NOP receptors in the brains of higher species are sparse, except for a single study in macaque central nervous system.[18] This study found a distribution of NOP quite similar to that in rat but with some definite differences. Receptor densities of > 6 fmol/mg (equating to > 6 nM in whole brain) were found in receptor-rich regions, such as cortex, caudate and amygdala. Thus, prospective PET radioligands for brain NOP receptors should have high affinity with a K_d value in the low nanomolar range.

The aforementioned autoradiographic studies were performed with peptide-like radioligands which would not be expected to enter brain freely. Intense effort has been expended over recent years to discover non-peptide small molecule ligands with high affinity as potential NOP receptor-targetted therapeutics.[19] A published example arising from this effort is SB-612111 (**1**; [(–)-*cis*-1-methyl-7-[[4-(2,6-dichlorophenyl)piperidin-1-yl]methyl]-6,7,8,9-tetrahydro-5*H*-benzocyclohepten-5-ol) (Chart 1).[20,21] From our own medicinal chemistry effort, we discovered a new series of high-affinity small molecule NOP receptor ligands, based on a 3-(2'-fluoro-4',5'-dihydrospiro[piperidine-4,7'-thieno[2,3-*c*]pyran]-1-yl)-2(2-

halobenzyl)-*N*-alkylpropanamide scaffold, which we disclose here. In this study, we explored this chemotype for the development of a PET radioligand for the NOP receptor, initially through screening of non-radioactive ligands in rat with ex vivo LC-MS/MS measures[22,23], and then through evaluation of selected ^{11}C-labeled ligands in rhesus monkey with PET. A promising NOP radioligand, [^{11}C](***S***)-**10c**, was found, which now merits further evaluation in human subjects.

Results and Discussion

Chemistry

The syntheses of the potential NOP ligands are outlined in Scheme 1. The spiro[4,5-dihydrothieno[2,3-*c*]pyran-7,4'-piperidine] **2** was synthesized from 2-(3-thienyl)ethanol by treatment of *t*-butylcarbonyl-protected (Boc-protected) piperidin-4-one in the presence of trifluoroacetic acid (TFA) in good yield. After the piperidine nitrogen was protected with Boc, fluorine was selectively introduced at the C2 position of the thienopyranyl ring via metallation with *n*-BuLi and subsequent reaction with the fluorination reagent *N*-fluoro-*N*-(phenylsulfonyl)benzenesulfonamide (NFSI) in 40–50% yield. Michael addition between the piperidine intermediate **5** and *t*-butyl acrylate under mild conditions gave the common intermediate propanoate **6** in 65% yield. α-Alkylation of propanoate **6** with either 2-fluoro-benzyl bromide or 2-chloro-benzyl bromide was achieved with LiN(TMS)$_2$ as base. Ester hydrolysis of compounds **7a** and **7b**, followed by conventional amide formation with the appropriate amine afforded the final amides **9a–c** and **10a–c**, which were each separated into enantiomers with chiral HPLC. The biologically active enantiomer of **9c** was determined by single-crystal X-ray crystallography to have *S*-configuration (see Supporting Information). The *R*-enantiomer of **9c** has markedly lower affinity (Table 1). The biologically less active enantiomer of **9a** was also determined by single-crystal X-ray crystallography to have *R*-configuration (see Supporting Information). We therefore reasoned that the higher affinity enantiomers of the NOP ligands **9a**, **9b**, and **10a–c** also have *S*-configuration

To assess the stereochemical stability of the chiral center in the new ligands, as well as explore possible future conditions of radiolabeling with [^{11}C]methyl iodide, compound (***S***)-**9a** was treated with sodium hydride in dimethyl sulfoxide (DMSO) solution at ambient temperature and then with methyl iodide. Chiral HPLC showed that this gave a single enantiomer of the *N*-methylated product **10a**, plus unchanged starting material, (***S***>)-**9a**. Therefore, these basic alkylation conditions do not cause significant racemization and the obtained product also has *S*-configuration (i.e., the product is (***S***)-**10a**).

Ligand Lipophilicity—Consideration of ligand lipophilicity is important in the development of PET radioligands. Moderate lipophilicity is usually sought to promote measurable plasma free fraction (f_P) and adequate brain entry, avoid excessive non-specific binding to brain tissue, and avoid the generation of lipophilic brain-penetrant radiometabolites.[10,13,24] The lipophilicity (*LogD*) of (***S***)-**10c** was measured to be 3.41 by a radiometric method and 3.50 by a shake-flask method (Table 1). This lipophilicity is within a range that is considered favorable for achieving adequate brain entry of a PET radioligand from blood without incurring excessive non-specific binding to brain tissue.[10,13,24] For ligands **10a–c**, the calculated lipophilicities (c*LogD* values at pH 7.4) were only slightly lower than those measured, so indicating that the computation on this type of structure was quite accurate. As expected, from the extra presence of an iso-propyl group, the c*LogD* and measured *LogD* values of ligand **10a** were appreciably higher than those of **10c**, as where those of **10b** in which a fluoro substituent of **10c** is replaced with a chloro substituent. The corresponding desmethyl compounds were computed to have less lipophilicity, as would also be expected.

Ligand Pharmacology—Ligands (***S***)-**10a–c** were found to have high binding affinity to human recombinant NOP receptors as represented by sub-nM K_i values in a binding assay with [^{3}H]nociceptin as reference NOP radioligand (Table 1). In a functional assay of receptor-mediated G-protein activation with [^{35}S]GTPγS, these ligands were each found to be potent antagonists at NOP receptors with sub-nM K_b values (Table 1). Thus, (***S***)-**10a–c** meet the high-affinity criterion previously mentioned for prospective NOP PET radioligands. The *R*-enantiomers were found to have substantially lower binding affinities and antagonist activities. Eudismic ratios ranged from 35 to 115. The enantiomers of the corresponding *N*-desmethyl ligands, **9a–c**, showed a similar pattern of binding affinity and antagonist activity and displayed eudismic ratios ranging from 20 to 169 (Table 1).

Studies in Rats—Initially, we applied our previously published in vivo/ex vivo LC-MS/MS method to characterize NOP ligands as potential tracers in rats, since this method avoids the need to use radiolabels.[22,23] Essentially, a low amount of non-radioactive ligand was injected intravenously into a group of rats, and after a set time the animals were sacrificed. Brain tissue regions, corresponding to high NOP and low NOP receptor expression, namely hypothalamus and striatum, respectively,[15,16] were dissected out and their concentrations of ligand measured with LCMS/MS. As a result, we identified three high-affinity ligands, (***S***)-**10a–c**, with potential for labeling to produce effective PET radioligands for brain NOP receptors. After intravenous administration into non-anesthetized rat, all three ligands showed quite fast kinetics with rapid and high rat brain uptake and washout occurring within one hour, a time-span consistent with the prospective use of short-lived carbon-11 as a radiolabel (Figure 1). Each ligand showed high brain uptake with ligand (***S***)-**10a** having slightly higher uptake (453% SUV at 10 min) than (***S***)-**10b** or (***S***)-**10c** (each ~ 280% SUV). All three ligands robustly demonstrated about three-fold higher uptake in NOP-rich hypothalamus than in NOP-poor striatum by 40 min after injection, thereby indicating a sizeable amount of NOP-receptor specific binding. Ligand (***S***)-**10b** had the largest ratio of NOP receptor-specific to non-specific binding (i.e., hypothalamus/striatum ligand concentration ratio minus 1 at 40 min), with a value of 3.5, whereas ligands (***S***)-**10a** and (***S***)-**10c** had ratios of 2.7 and 2.3, respectively. These ratios are in fact under-estimates of specific to non-specific binding in hypothalamus because rat striatum is not entirely devoid of NOP receptors.[15,16]

Radioligand Syntheses—Ligands (***S***)-**10a–c** and (***R***)-**10c** were rapidly labeled with carbon-11 by treating their respective *N*-desmethyl precursors, (***S***)-**9a–c** and (***R***)-**9c**, with [^{11}C]methyl iodide in the presence of KOH as base (Scheme 2). The radioligands were isolated with reverse phase HPLC in useful activities (mean yields for $n = 3$ were 47, 75 and 85 mCi for [^{11}C](***S***)-**10a–c**, respectively), and in high radiochemical purities (> 99%) and specific radioactivities (mean values for $n = 3$ were, 7.8, 5.1, 3.6 Ci/μmol at end of synthesis for [^{11}C](***S***)-**10a–c**, respectively). Chiral HPLC analyses of the radioligands verified almost complete absence of racemisation in the labeling procedure (see Supporting Information for chiral HPLC analysis of [^{11}C](***S***)-**10c**). Each radioligand was readily formulated in ethanol (10% v/v)-saline for intravenous administration into monkey. Each was radiochemically stable in formulation medium. The radiosyntheses times were about 45 min from the end of radionuclide production.

PET Imaging in Monkeys—After intravenous administration into monkey, each high-affinity radioligand, [^{11}C](***S***)-**10a–c**, showed similar brain radioactivity kinetics, characterized by rapid high uptake into brain followed by progressive washout of radioactivity from all examined regions over the duration of the scanning session (either 90 or 120 min) (Figure 2). Cerebellum showed highest initial uptake and fastest washout of radioactivity in each case, possibly due to greater regional blood flow in this region of brain

during anesthesia. The rank order of initial radioactivity uptake was [^{11}C](***S***)-**10c** > [^{11}C](***S***)-**10b** > [^{11}C](***S***)-**10a**. [^{11}C](***S***)-**10c** also gave the greatest separation of time-activity curves across brain regions. Compound **1** is a highly potent (Table 1) and selective antagonist for NOP receptors, showing more than 1000-fold lower affinity for classical opioid receptors.[21] In corresponding experiments in which brain NOP receptors were pre-blocked by administration of **1**, brain radioactivity kinetics were altered in a consistent manner (Figure 2). Thus, in each monkey, maximal initial radioactivity uptake was again high, but was followed by a much faster washout of radioactivity from all examined brain regions than in the corresponding baseline scans, and with very little separation in the time-activity curves for noncerebellar regions. Such differences in kinetics imply the presence of a significant proportion of NOP receptor-specific binding of the radioligand in the baseline experiments. Major differences were also clearly apparent in the PET images obtained under baseline and pre-block conditions. Thus, the baseline experiments showing a regional distribution of radioactivity reflecting the distribution of NOP receptors expected from the autoradiographic study in macaque brain[18], with, for example, high uptake in caudate and relatively low uptake in hypothalamus – the reverse of relative levels in rat[15,16]. The pre-block experiments in monkey showed low and uniform distributions of radioactivity consistent with non-specific binding of radioligand and/or radiometabolites. These image differences are exemplified in Figure 3 for [^{11}C](***S***)-**10c**.

Comparison of the areas-under-the-curves (AUCs) between baseline and pre-block PET experiments provided further evidence for an appreciable proportion of NOP receptor-specific binding under baseline conditions. Thus, for each radioligand, the brain-averaged AUCs (%SUV × min) between 0 and 90 min or between 30 and 90 min were appreciably greater in the baseline experiments than in the pre-block experiments. From these data, crude estimates of ratios of NOP receptor-specific binding to non-specific binding were derived as $[(AUC_{baseline}/AUC_{pre\text{-}block})-1]$ for the time intervals 0–90 and 30–90 min after radioligand injection. These estimates (Table 2) confirm that each radioligand produced a high proportion of NOP receptor-specific binding in baseline PET scans, with radioligands [^{11}C](***S***)-**10b** and [^{11}C](***S***)-**10c** showing appreciably higher proportions than [^{11}C](***S***)-**10a**.*

Radioligand [^{11}C](***S***)-**10c** was selected for deeper investigation because of its high brain uptake and apparently high ratio of NOP-receptor specific to non-specific binding. Administration of the selective NOP ligand **1** to monkey at 40 min after [^{11}C](***S***)-**10c** resulted in a faster washout of radioactivity from all brain regions down to a low level, so demonstrating the reversibility of the specific binding of [^{11}C](***S***)-**10c** to NOP receptors (Figure S4, Supporting Information). The opiate receptor antagonist naloxone is effective at displacing opiate receptor radioligands from primate brain.[25,26] In another monkey PET experiment, administration of a high dose of naloxone at 37 min after [^{11}C](***S***)-**10c** had no effect on the washout of radioactivity from brain, thereby showing that this radioligand does not bind significantly to opiate receptors (Figure S5, Supporting Information). Furthermore, baseline and pre-block experiments in a single monkey with [^{11}C](***R***)-**10c**, the lower affinity enantiomer of [^{11}C](***S***)-**10c**, provided no evidence of receptor-specific binding, since they showed similar fast kinetics in all brain regions with no separation of regional time-activity curves (Figure S6, Supporting Information). Maximal brain radioactivity uptake was in fact higher in the pre-block experiment.

Emergence of Radiometabolites of [^{11}C](*S*)-10c in Monkey Plasma In Vivo—

Generally, PET radioligands are appreciably metabolized over the short time-span of a PET scanning session. Detailed quantitative analysis of radioligand behavior in vivo to derive

*A full bio-mathematical compartmental analysis of monkey PET scans to derive accurate binding potentials is beyond the scope of this report and will be published subsequently.

important output measures such as binding potential or volume of distribution may require accurate measurement of f_P and also the determination of how the amount of unmetabolized radioligand in plasma changes over the full duration of a scanning session (the radioligand arterial input function). Generally, PET radioligands that produce appreciable amounts of brain-penetrant radiometabolites are difficult to quantify.

[^{11}C](***S***)-**10c** was found to be radiochemically stable (98.9 ± 0.4% unchanged, n = 4) in sodium phosphate buffer (0.15 M, pH 7.4) for 2.5 h, and also stable in monkey blood and plasma for 0.5 h at room temperature [100.4 ± 0.01% (n = 6) and 99.9 ± 0.01% (n = 6)]. The f_P value of [^{11}C](***S***)-**10c** in monkey blood in vitro was quite low (11.3 ± 1.1%; n = 6, 3 samples from each of 2 monkeys) but readily measurable with good accuracy. The f_P value in human pooled plasma was similar to that in the monkey (11.0 ± 0.7%; 3 samples from each of 2 subjects). The values are within the range expected for the lipophilicity of (***S***)-**10c** (*LogD* = 3.41).[27]

After administration of [^{11}C](***S***)-**10c** into monkey, both the total radioactivity in plasma and the parent radioligand component reduced rapidly (Figure 4). Recoveries of radioactivity from plasma into supernatant acetonitrile for HPLC analysis were 94.9 ± 3.3% (n = 106). HPLC analyses of plasma from monkeys studied at baseline revealed [^{11}C](***S***)-**10c** eluting at 4.4 ± 0.8 min (n = 100), and three less lipophilic radiometabolites eluting at 1.7 ± 0.4, 2.2 ± 0.5 and 2.7 ± 0.6 min (n = 100), respectively. [^{11}C](***S***)-**10c** was rapidly metabolized to a virtually equal extent in both baseline and pre-block experiments in the same monkeys, respectively (Figure 5). The identities of the three radiometabolites are currently unknown, as is their ability to penetrate the blood-brain barrier. Their lower lipophilicities relative to that of [^{11}C](***S***)-**10c**, as deduced from their shorter retention times on reverse phase HPLC, might render them less brain-penetrant and untroublesome to quantitative analysis. As shown in Figure 2, treatment of monkey with the NOP antagonist **1** before [^{11}C](***S***)-**10c** resulted in a continuous decline of radioactivity in all brain regions to a low level, representing about 15% of the early peak value at the end of the scanning session (~ 120 min). Radiometabolites are therefore unlikely to be entering brain to a troublesome extent.†

Test of Radioligand Selectivity by In vitro Autoradiography of Wild-type and NOP Knockout Mouse Brain—Autoradiographs of post mortem wild-type mouse brain slices with [$^{3}H_3$](***S***)-**10c** showed a discrete distribution of radioligand uptake (Figure 6), and they were very comparable with those previously reported for rat using [^{3}H]nociceptin[15] or other peptide-like NOP receptor radioligands.[14,16,17] [$^{3}H_3$](***S***)-**10c** gave only low non-specific binding. Autoradiographs in NOP receptor knockout mice showed only a very low uniform distribution of [^{3}H](***S***)-**10c**, so demonstrating the specificity of the binding of this radioligand to NOP receptors in wild-type mouse brain.

Summary

The 3-(2'-fluoro-4',5'-dihydrospiro[piperidine-4,7'-thieno[2,3-*c*]pyran]-1-yl)-2(2-halobenzyl)-*N*-alkylpropanamides represent a new chemotype of high-affinity NOP receptor ligand. This study shows that this chemotype is suitable for the developent of prospective NOP receptor PET radioligands, of which [^{11}C](***S***)-**10c**, on account of its good brain entry, favorable kinetics and strong receptor-specific signal in rat and monkey in vivo, is particularly promising for further evaluation in human subjects.

†Our detailed kinetic analysis of [^{11}C](***S***)-**10c** in monkey, to be published elsewhere, show that stable volumes of distribution values are established rapidly, and therefore that radiometabolites do not enter brainly to be problematic to receptor quantification.

Experimental Section

Materials and Methods—All reagents used were obtained from commercial sources (Sigma-Aldrich, unless otherwise stated). All solvents were of an analytical grade. The NOP ligand, **1**[20,21], used as a NOP blocking or NOP ligand displacing compound, was synthesized at Eli Lilly and Company. [^{3}H](***S***)-**10c** was prepared by treating the *N*-desmethyl compound (***S***)-**9c** with [$^3H_3$]methyl iodide and obtained in > 99% radiochemical purity, as determined with HPLC on a reverse phase C18 column (5 μm; 4.6 × 150 mm) eluted with a mixture of 0.05% TFA (A) and MeCN (B) at 1 ml/min with B increased from 30% v/v/ to 90% at 10 min and returned to 30% at 12 min (t_R = 7.89 min). The specific activity of [^{3}H](***S***)-**10c** was found to be 53 Ci/mmol with mass spectrometry. [^{35}S]GTPγS was obtained commercially.

Isolation of compounds by column chromatography was performed on silica gel columns (SP1a HPFC system, Biotage Inc., Charlottesville, VA).

^{1}H NMR (300 MHz) spectra were acquired at 20 °C on a System 300 instrument (Varian; Palo Alto, CA). Abbreviations s, d, dd, ddd, m, and br denote singlet, doublet, double doublet, double double doublet, multiplet, and broad, respectively.

LC-MS was performed with an 1100 Series LC-MSD single quadrupole instrument (Agilent; Santa Clara, CA) with an ESI interface. Samples were analyzed by method 1, 2 or 3. Method 1, used a heated (50 °C) Gemini C18 column (3.0 μm; 2.0 × 50 mm; Phenomenex, Torrance, CA) eluted at 1 mL/min with a gradient of A (H_2O containing 0.01%TFA) and B (MeCN containing 0.01% TFA) with B increased linearly from 5 to 100% (v/v) over 7 min and then held for 1 min. Method 2, analyses used a heated (50 °C) Gemini C18 column (3.0 μm; 2.0 × 50 mm) eluted at 1 mL/min with a gradient of A (aq. NH_4HCO_3; 10 mM) and B (MeCN), with B increased linearly from 10 to 100% (v/v) over 7 min and then held for 1 min. Method 3used an XBridge C18 column (3.5 μm; 2.1 × 50 mm; Waters, Milford, MA) eluted at 1 mL/min with a gradient of A (aq. NH_4HCO_3; 10 mM, pH 9) and B (MeCN), with B increased linearly from 10 to 100% (v/v) over 7 min and then held for 1 min. Ions between m/z 80 and 800 were captured after electrospray ionization of the eluted test sample. The purities of synthesized ligands were all found to be ≥ 95%, by methods 1, 2 or 3 as specified later..

High-resolution mass spectrometry (HRMS) was performed on an TOF/Q-TOF instrument (Agilent). Data were acquired in dual ESI mode (+ and −) in the range of 95–1700 amu. The sample (~ 0.1 mg/mL in MeCN-H_2O, 1: 1 v/v; 2 μL) was injected in loop mode onto a Zorbax SBC8 column (3.5 μm; 3.0 × 150 mm; Agilent) eluted at 0.5 mL/min with a mixture of 0.1% formic acid in water (A) and 0.1% formic acid in MeCN (B) with B increasing from 5 to 100% over 15 min and then then held at 100% for 8 min. Eluate was monitored with a diode array detector oprating in the range 190 to 700 nm.

Melting points (mp) were determined on a DSC Q100V9.8 instrument (Universal) with a ramp of 5°C/min up to 300°C, and were uncorrected.

Optical rotations were measured with a 341 polarimeter (Perkin Elmer) at 20 °C and at 589 nm (sodium lamp).

γ-Radioactivity from carbon-11 was measured using a calibrated dose calibrator (Atomlab 300; Biodex Medical Systems; Shirley, NY). Radioactivity measurements were corrected for physical decay. All radiochemistry with carbon-11 was performed in a lead-shielded hot-cell for personnel protection from radiation.

Statistics—Values are given as means ± the standard deviation of the mean, unless otherwise stated.

Animals—Male Sprague-Dawley rats (Harlan Sprague-Dawley, Indianapolis, IN), weighing between 230 and 280 g, were used for in vivo experiments. All rats were housed in rooms using a 12-hour light/dark cycle and had ad lib access to normal rat chow and water until the beginning of the 3-h experimental protocol. All experiments with rats were performed in accord with the National Research Council Guide under protocols approved by the Animal Care and Use Committee of Eli Lilly and Company.

All rhesus (*Mucacca mulatto*) monkeys were handled in accordance with the *Guide for the Care and Use of Laboratory Animals*[28] and the National Institute of Health Animal Care and Use Committee.

Chemistry

Spiro[4,5-dihydrothieno[2,3-*c*]pyran-7,4'-piperidine], (2)—2-(Thiophen-3-yl)ethanol (15.4 g, 120 mmol) was added to a solution of *N*-*t*-butoxycarbonyl-4-piperidone (20 g, 100 mmol) in CH_2Cl_2 (200 mL) at room temperature (r.t.). TFA (38 mL) was added dropwise to the mixture over 30 min while the internal temperature was kept between 23 and 30°C. The mixture was then stirred at r.t. for 20 h. Solvent was then evaporated off and the residue was poured into NaOH (1M; 200 mL). The mixture was stirred for 15 min and the pH adjusted to about 11 with 50% aq. NaOH. Then the mixture was extracted with CH_2Cl_2. The organic layers were separated, dried over Na_2SO_4 and evaporated. The crude residue was purified on silica gel (CH_2Cl_2: MeOH; 20: 1 v/v) to afford 19.9 g (95%) of **2** as a solid; LC-MS (ESI) *m/z* 210 $(M+H)^+$, purity 100%, t_R = 1.68 min, method 2; ^{1}H-NMR (300 MHz, $CDCl_3$): δ7.14 (d, *J* = 4.8 Hz, 1H), 6.77 (d, *J* = 5.1 Hz, 1H), 3.93 (t, *J* = 5.4 Hz, 2H), 3.09 (td, *J* = 3.0 Hz, 12.3 Hz, 2H), 2.98−2.92 (m, 2H), 2.70 (t, *J* = 5.7 Hz, 2H), 2.01−1.99 (m, 2H), 1.86 (td, *J* = 4.5 Hz, 12.3 Hz, 2H).

***t*-Butyl spiro[4,5-dihydrothieno[2,3-*c*]pyran-7,4'-piperidine]-1-carboxylate, (3)—**Triethylamine (TEA, 0.97 g, 9.56 mmol) was added to a mixture of **2** (1.0 g, 4.78 mmol) and *di*-*t*-butyl dicarbonate (1.25 g, 5.74 mmol) in dry dichloromethane (20 mL), and stirred at r.t. for 5 h. The reaction mixture was then washed with 1M HCl and brine, dried over Na_2SO_4, filtered, and concentrated in *vacuo* to afford **3** as a yellow oil (1.476 g, 100%); LC-MS (ESI): *m/z* 210 $(M+H-100)^+$, purity 100%, t_R = 1.82 min, method 1; ^{1}H-NMR (300 MHz, $CDCl_3$) δ7.14 (d, *J* = 4.8 Hz, 1H), 6.77 (d, *J* = 5.1 Hz, 1H), 4.05−3.91 (m, 4H), 3.21−3.05 (m, 2H), 2.70 (t, *J* = 5.4 Hz, 2H), 2.00−1.96 (m, 2H), 1.80 (td, *J* = 5.1 Hz, 12.9 Hz, 2H), 1.52 (s, 9H).

t*-Butyl 2-fluorospiro[4,5-dihydrothieno[2,3-*c*]pyran-7,4'-piperidine]-1'-carboxylate, (4)—n*-BuLi (1.6 M; 10.7 mmol) in hexane (6.7 mL) was added dropwise to a solution of **3** (1.102 g, 3.57 mmol) in dry THF (15 mL) at −78 °C under N_2. The reaction mixture was stirred at −78 °C for 1 h, and then a solution of NFSI (2.811 g, 8.93 mmol) in dry THF (30 mL) was added at −78 °C. The mixture was then warmed to r.t. and stirred overnight. The reaction was quenched with saturated NH_4Cl solution, and the mixture extracted with EtOAc. The organic layer was washed with brine, dried over Na_2SO_4, and concentrated in *vacuo*. The residue was purified by column chromatography (petroleum ether: CH_2Cl_2; 2: 1 v/v), and then HPLC on a Discovery C18 column (5 μm; 21.2 × 150 mm; Waters Corp.) eluted with 0.005% TFA in water-MeCN as mobile phase at 24 mL/min to afford **4** ($t_{\mathbf{R}}$ = 7.8−8.3 min) as a yellow oil (510 mg, 43.7%); LC-MS (ESI): *m/z* 228 $(M+H-100)^+$, purity 100%, $\boldsymbol{t_R}$ = 2.90 min, method 2; ^{1}H-NMR (300 MHz, $CDCl_3$) δ 6.13 (d, *J*

= 1.5 Hz, 1H), 4.03−3.90 (m, 4H), 3.17−3.02 (m, 2H), 2.56 (t, *J* = 5.1 Hz, 2H), 2.02−1.93 (m, 2H), 1.72−1.60 (m, 2H), 1.47 (s, 9H).

2-Fluorospiro[4,5-dihydrothieno[2,3-*c*]pyran-7,4'-piperidine], (5)—HCl (4M; 13.6 mmol) in dioxane, (3.4 mL) was added to a solution of **4** (510 mg, 1.56 mmol) in CH_2Cl_2 (3 mL). The reaction mixture was stirred for 3 h, diluted with CH_2Cl_2 and then washed with water and brine. The organic phase was dried over Na_2SO_4, filtered and concentrated in vacuo to afford **5** as a yellow solid (278 mg, 78%); LC-MS (ESI): *m/z* 228 $(M+H)^+$, purity 93.8%, t_R = 1.99 min, method 2; ^{1}H-NMR (300 MHz, $CDCl_3$) δ 6.12 (s, 1H), 3.92 (t, *J* = 5.7 Hz, 2H), 3.70 (s, 1H), 3.04−2.89 (m, 4H), 2.54 (t, *J* = 5.7 Hz, 2H), 2.02−1.97 (m, 2H), 1.72 (td, *J* = 13.2 Hz, 4.8 Hz, 2H).

***t*-Butyl 3-(2-fluorospiro[4,5-dihydrothieno[2,3-*c*]pyran-7,4'-piperidine]-1'-yl)propanoate, (6)—**A mixture of **5** (278 mg, 1.22 mmol), *t*-butyl acrylate (313 mg, 2.45 mmol) and TEA (367 mg, 3.67 mmol) in THF (10 mL) was heated to 65 °C, and stirred for 20 h. The reaction mixture was then cooled to r.t. and concentrated in *vacuo*. The residue was dissolved in CH_2Cl_2 and washed with 1.0 M HCl (aq.) and brine. The organic layer was dried over Na_2SO_4, filtered and concentrated in *vacuo*. The residue was purified by TLC (petroleum ether: EtOAc; 1: 1 v/v) to afford **6** as a yellow oil (285 mg, 65.8%); LC-MS (ESI): *m/z* 356 (M+H)+, purity 100%, t_R = 2.30 min, method 2; ^{1}H-NMR (300 MHz, $CDCl_3$) δ 6.11 (d, *J* = 2.1 Hz, 1H), 3.91 (t, *J* = 5.4 Hz, 2H), 2.73−2.68 (m, 4H), 2.54 (t, *J* = 5.4 Hz, 2H), 2.46−2.41 (m, 4H), 2.04−1.98 (m, 2H), 1.81 (td, *J* = 13.5, 4.5 Hz, 2H), 1.46 (s, 9H).

***t*-Butyl 2-[(2-fluorophenyl)methyl]-3-(2-fluorospiro[4,5-dihydrothieno[2,3-*c*]pyran-7,4'-piperidine]-1'-yl)propanoate, (7a)—**A 1M solution of $LiN(TMS)_2$ (2.70 mmol) in THF (2.70 mL) was added dropwise to a stirred solution of **6** (318 mg, 0.90 mmol) in dry THF (20 mL) at −78 °C. The mixture was stirred for 1 h at the same temperature. 1,3-Dimethyl-tetrahydropyrimidin-2(1*H*)-one (92 mg, 0.72 mmol) in dry THF (10 mL) was added at −78 °C and stirred for 30 min. To the resulting mixture was added 1-(bromomethyl)-2-fluorobenzene (141 mg, 0.75 mmol) in dry THF (10 mL) at −78 °C. Stirring was continued for 1 h and then the temperature allowed to rise to 0 °C where it was kept for 1 h. The reaction mixture was quenched with saturated NH_4Cl solution and twice extracted with EtOAc. The organic layers were combined and washed with brine, dried over Na_2SO_4, and concentrated. The residue was purified by TLC (petroleum ether: EtOAc; 8: 1 v/v) to afford **7a** as a yellow oil (341 mg, 82.8%); LC-MS (ESI): *m/z* 464 (M+H)+, purity 91.6%, t_R = 2.63 min, method 2; ^{1}H-NMR (300 MHz, $CDCl_3$) δ 7.22−7.14 (m, 2H), 7.06−6.90 (m, 2H), 6.11 (d, *J* = 1.5 Hz, 1H), 3.90 (t, *J* = 5.1 Hz, 2H), 2.98−2.30 (m, 11H), 2.03−1.91 (m, 2H), 1.80−1.65 (m, 2H), 1.34 (s, 9H).

***t*-Butyl 3-(2-fluorospiro[4,5-dihydrothieno[2,3-*c*]pyran-7,4'-piperidine]-1'-yl)propanoate, (7b)—**Compound **6** (0.83 g, 2.33) was dissolved in dry THF (15 mL) and then cooled to −78 °C. The solution was purged with nitrogen three times. $LiN(TMS)_2$ (7.0 mL, 7.00 mmol) was added dropwise to the reaction at −78 °C and the mixture was stirred at this temperature for 1.5 h. A solution of 1,3-dimethyl-3,4,5,6-tetrahydro-2(1*H*)-pyrimidinone (0.24 g, 1.87 mmol) in THF (5 mL) was added dropwise and the reaction mixture was stirred for 0.5 h at −78 °C. Then a solution of 1-(bromomethyl)-2-chlorobenzene (0.72 g, 3.50 mmol) in THF (5 mL) was added. The mixture was stirred at −78 °C for 0.5 h and then at 0 °C for 0.5 h. The reaction was quenched by adding saturated aq. NH_4Cl. The aqueous phase was extracted with EtOAc and then discarded. The organic phase was dried over Na_2SO_4 and concentrated. TLC (petroleum ether: EtOAc; 10: 1 v/v) of the crude product gave **7b** as a solid (1.1 g, 98% yield); LC-MS (ESI): *m/z*: 480 $(M+H)^+$,

purity 95.2%, t_R = 2.77 min, method 2; ^{1}H-NMR (300 MHz, $CDCl_3$): δ 7.34−7.13 (m, 4H), 6.10 (s, 1H), 3.89 (t, *J* = 5.4 Hz, 2H), 3.05−2.29 (m, 11H), 2.01−1.90 (m, 2H), 1.80−1.65 (m, 2H), 1.34 (s, 9H).

2-[(2-Fluorophenyl)methyl]-3-(2-fluorospiro[4,5-dihydrothieno[2,3-*c*]pyran-7,4'-piperidine]-1'-yl)propanoic acid, (8a)—Compound **7a** (1.53 g, 3.29 mmol) was dissolved in dry CH_2Cl_2 (5 mL) and TFA (10 mL) was added. The mixture was stirred at r.t. for 16 h. Solvent was removed to give **8a** as a yellow oil (1.33 g). The crude material was used in subsequent steps without further purification; LC-MS (ESI): 408 $(M+H)^+$, purity 94.5%, t_R = 1.74 min, method 2,.

2-[(2-Chlorophenyl)methyl]-3-(2-fluorospiro[4,5-dihydrothieno[2,3-*c*]pyran-7,4'-piperidine]-1'-yl)propanoic acid, (8b)—Compound **7b** (1.10 g, 2.29 mmol) was dissolved in dry CH_2Cl_2 (30 mL) and TFA (3 mL) was added. The mixture was stirred at r.t. for 5 h. The solvent was removed to give crude **8b** (0.97 g) which was used in subsequent steps without further purification; LC-MS (ESI): 424 $(M+H)^+$, purity 98%. t_R = 2.07 min, method 2

(2*S*)-2-[(2-Fluorophenyl)methyl]-3-(2-fluorospiro[4,5-dihydrothieno[2,3-*c*]pyran-7,4'-piperidine]-1'-yl)-*N*-isopropyl-propanamide, ((*S*)-9a)—Di-isopropylethylamine (DIPEA; 1.29 g, 9.984 mmol) was added to a solution of **8a** (0.68 g, 1.677 mmol) in CH_2Cl_2 (20 mL), followed by 2-propanamine (0.39 g, 6.6 mmol), 1-ethyl-3(dimethylaminopropyl)-carbodiimide (EDCI) hydrochloride (0.64 g, 3.34 mmol), and 1-hydroxybenzotriazole (HOBt, 0.45 g, 3.33 mmol). The reaction mixture was stirred at r.t. overnight, diluted with CH_2Cl_2 (50 mL), washed with $NaHCO_3$ (aq.) and brine, dried over Na_2SO_4, and evaporated to dryness. The residue was purified with TLC (CH_2Cl_2: MeOH; 25: 1 v/v) to afford **9a** (0.65 mg, 88.06%). LC-MS ESI m/z: 449 $(M+1)^+$, purity 98%, t_R = 5.05 min, method 2 . Chiral HPLC of **9a** on a Chiralpak AD column: (10 μm; 4.6 × 250 mm) eluted with hexane containing dimethylethylamine (DMEA; 0.2%) and EtOH (5%) at 1 mL/min, gave (***S***)-**9a** as a solid (268 mg): t_R = 7.34 min; m.p.: 139.0−139.9 °C; $[\alpha]_D$ = −7.8° (*c*. 8.2 MeOH); ^{1}H-NMR (300 MHz, MeOH-d_4): δ 7.23−7.18 (m, 2H), 7.08−7.00 (m, 2H), 6.22 (s, 1H), 3.92−3.83 (m, 3H), 2.89−2.65 (m, 6H), 2.54−2.32 (m, 5H), 1.99−1.94 (m, 2H), 1.81−1.70 (m, 2H), 1.18 (d, *J* = 6.6 Hz, 3H), 1.00 (d, *J* = 6.6 Hz, 3H); LC-MS (ESI): m/z 449.2 $(M+1)^+$, purity 100%, t_R = 4.21 min, method 3; HRMS (ESI): calc'd for $C_{24}H_{30}F_2N_2O_2S+H^+$, 448.2069, found 448.2073.

(2*R*)-2-[(2-Fluorophenyl)methyl]-3-(2-fluorospiro[4,5-dihydrothieno[2,3-*c*]pyran-7,4'-piperidine]-1'-yl)-*N*-isopropyl-propanamide, ((*R*)-9a)—The chiral HPLC of **9**, described above, also gave (***R***)-**9a** as a solid (271 mg): t_R = 9.26 min; m.p.: 137.3−139.1 °C; $[\alpha]_D$ = +8.2° (*c*. 11.1 MeOH); ^{1}H-NMR and LC-MS as for (***S***)-**9**, purity 100%, t_R = 4.21 min, method 3; HRMS (ESI) calc'd for $C_{24}H_{30}F_2N_2O_2S+H^+$, 448.2069, found 448.2075.

(2*S*)-2-[(2-Chlorophenyl)methyl]-3-(2-fluorospiro[4,5-dihydrothieno[2,3-*c*]pyran-7,4'-piperidine]-1'-yl)propanamide, ((*S*)-9b)—DIPEA (0.89 g, 6.85 mmol) was added to a solution of **8b** (0.48 g, 1.14 mmol) in CH_2Cl_2 (20 mL) followed by NH_4Cl (0.18 g, 3.34 mmol), EDCI hydrochloride (0.44 g, 2.28 mmol) and HOBt (0.31 g, 2.28 mmol). The reaction mixture was stirred at r.t. overnight, diluted with CH_2Cl_2 (50 mL), washed with $NaHCO_3$ (aq.) and brine, dried over Na_2SO_4, and evaporated to dryness. The residue was purified with TLC (CH_2Cl_2: MeOH, 5: 1 v/v) to afford **9b** (250 mg, 52%). Chiral HPLC of **9b** on a Daicel AD-H column (5 μm; 21.2 × 250 mm) eluted at 12 mL/min with A: B (90: 10 v/v) (A: 0.1% diethylamine (DEA) in hexane, and B: 0.1% DEA in EtOH)

with eluate monitored for absorbance at 214 nm gave (***S***)-**9b** (80 mg; t_R = 13.29 min); m.p.: 127.5−130.1 °C; $[\alpha]_D$ = −12.7° (*c*. 10.0 MeOH); LC-MS (ESI): m/z: 423 $(M+H)^+$, purity: 99%, t_R = 4.59 min, method 2. ^{1}H-NMR (300 MHz, $CDCl_3$) δ 7.64 (brs, 1H), 7.35−7.24 (m, 2H), 7.21−7.12 (m, 2H), 6.11 (d, J = 1.2 Hz, 1H), 5.25 (brs, 1H), 3.86 (t, J = 5.4 Hz, 2H), 3.35−3.26 (m, 1H), 2.89−2.61 (m, 5H), 2.54−2.44 (m, 3H), 2.41−2.36 (m, 1H), 2.24−2.12 (m,1H), 2.01−1.92 (m, 2H), 1.81−1.60 (m, 2H); HRMS (ESI): calc'd for $C_{21}H_{24}ClFN_2O_2S$ $+H^+$, 423.1304, found 423.1306.

(2*R*)-2-[(2-Chlorophenyl)methyl]-3-(2-fluorospiro[4,5-dihydrothieno[2,3-*c*]pyran-7,4'-piperidine]-1'-yl)propanamide, ((*R*)-9b)—The chiral HPLC of **9b** (90 mg), described above, also gave (***R***)-**9b** (t_R = 15.74 min; 90 mg); m.p.: 126.1−129.4 °C; $[\alpha]_D$ = +12° (*c*. 10.0 MeOH); ^{1}H-NMR and LC-MS, as for (***S***)-**9b**, purity 100%, t_R = 4.59 min, method 2; HRMS (ESI): calc'd for $C_{21}H_{24}ClFN_2O_2S+H^+$, 423.1304, found 423.1303.

(2*S*)-2-[(2-Fluorophenyl)methyl]-3-(2-fluorospiro[4,5-dihydrothieno[2,3-*c*]pyran-7,4'-piperidine]-1'-yl)propanamide, ((*S*)-9c)—Di-isopropylethylamine (DIPEA) (1.41 g, 10.9 mmol) was added to a solution of crude **8a** (0.74 g, 1.82 mmol) in CH_2Cl_2 (20 mL), followed by NH_4Cl (0.29 g, 5.54 mmol), EDCI hydrochloride (0.70 g, 3.63 mmol), and HOBt (0.49 g, 3.63 mmol). The reaction mixture was stirred at r.t. overnight. The mixture was then diluted with CH_2Cl_2 (50 mL), washed with $NaHCO_3$ (aq.) and brine, dried over Na_2SO_4, and evaporated to dryness. The crude material was purified with TLC (CH_2Cl_2: MeOH; 25: 1 v/v) to afford **9c** as a light yellow oil (0.5 g, 60% yield). Chiral HPLC of **9c** on a Daicel OJ-H column: (5 μm; 21.2 × 250 mm); eluted at 15 mL/min with A: B (80: 20 v/v) (A: 0.1% DEA/hexane; B: 0.1% DEA/alcohol) with eluate monitored for absorbance at 214 nm gave (***S***)-**9c** (0.230 g; t_R = 9.6 min); m.p.: 118.2−120.0 °C; $[\alpha]_D$ = +2.6° (*c*. 7.09 MeOH); ^{1}H-NMR (300 MHz, $CDCl_3$): δ 7.92 (brs, 1H), 7.25−7.14 (m, 2H), 7.10−6.95 (m, 2H), 6.10 (d, *J* = 1.5 Hz, 1H), 5.32 (brs, 1H), 3.88 (t, *J* = 5.4 Hz, 2H), 3.22 (d, *J* = 3.9 Hz, 1H), 2.82−2.58 (m, 5H), 2.57−2.44 (m, 3H), 2.36 (d, *J* = 3.0 Hz, 1H), 2.17 (t, *J* = 12.0 Hz, 1H), 2.01 (d, *J* = 13.5 Hz, 2H), 1.82−1.55 (m, 2H); LC-MS (ESI): *m/z*: 407 $(M+1)^+$, purity: 99%, t_R = 4.34 min, method 2; HRMS (ESI): calc'd for $C_{21}H_{24}F_2N_2O_2S+H^+$, 407.1599; found, 407.1602.

(2*R*)-2-[(2-Fluorophenyl)methyl]-3-(2-fluorospiro[4,5-dihydrothieno[2,3-*c*]pyran-7,4'-piperidine]-1'-yl)propanamide, ((*R*)-9c)—The chiral HPLC of **9c**, described above, also gave (***R***)-**9c** (0.21 g; t_R = 8.2 min); m.p.: 117.4–119.9 °C; $[\alpha]_D$ = −2.9° (*c*. 7.29 MeOH); ^{1}H-NMR and LCMS (ESI) as for (***S***)-**9c**; purity 100%, t_R = 4.3 min, method 2; HRMS (ESI): calc'd for $C_{21}H_{24}F_2N_2O_2S+H^+$, 407.1599, found 407.1600.

(2*S*)-2-[(2-Fluorophenyl)methyl]-3-(2-fluorospiro[4,5-dihydrothieno[2,3-*c*]pyran-7,4'-piperidine]-1'-yl)-*N*-isopropyl-*N*-methyl-propanamide, ((*S*)-10a)— DIPEA (0.74 g, 5.73 mmol) was added to a solution of **8a** (0.75 g, 1.84 mmol) in CH_2Cl_2 (50 mL), followed by *N*-methyl 2-propanamine, (0.280 g, 3.83 mmol), EDCI hydrochloride (0.71 g, 3.7 mmol) and HOBt (0.50 g, 3.70 mmol). The reaction mixture was stirred at r.t. overnight, diluted with CH_2Cl_2 (30 mL), washed with $NaHCO_3$ (aq) and brine, dried over Na_2SO_4, and evaporated to dryness. The residue was purified by chromatography to afford **10a** as an oil (0.654 g, 76.8%). Chiral HPLC on a Chiralpak AD column (10 μm; 4.6 × 250 mm) eluted with 10% hexane in 0.2% DMEA in EtOH at 1 mL/min gave (***S***)-**10a** as an oil (170 mg; t_R = 5.03 min); $[\alpha]_D$ = −16.5° (*c*. 7.9 MeOH); ^{1}H-NMR (DMSO-d_6, 300 MHz) δ (amide rotamers are observed) 7.27–7.14 (m, 2H); 7.11–7.05 (m, 2H); 6.44 (s, 1H); 4.64 and 4.03 (d *J* = 6 Hz, 1H); 3.83 (m, 2H); 3.25 (m, 1H); 2.83 (m, 1H); 2.59 (s, 3H); 2.72–2.23 (m, 9H); 1.92–1.81 (m, 2H); 1.61–1.52 (m, 2H); 1.15 and 0.99 (dd, *J* = 6 Hz, 3H); 0.85 and 0.75

(dd, *J* = 6 Hz, 3H); LC-MS (ESI): *m/z* 463.2 (M+H)+, purity 100%, t_R = 4.74, method 3; HRMS (ESI): calc'd for $C_{25}H_{32}F_2N_2O_2S+H^+$, 463.2225, found 463.2228.

(2*R*)-2-[(2-Fluorophenyl)methyl]-3-(2-fluorospiro[4,5-dihydrothieno[2,3-*c*]pyran-7,4'-piperidine]-1'-yl)-*N*-isopropyl-*N*-methyl-propanamide, ((*R*)-10a)— The chiral HPLC of **10a** described above also gave (***R***)-**10a** as an oil (191 mg; t_R = 6.40 min); $[\alpha]_D$ = +16.0° (*c*. 7.9 MeOH); ^{1}H-NMR and LC-MS (ESI) as for (***S***)-**10a**: purity 100%, t_R = 4.75 min, method 3; HRMS (ESI): calc'd for $C_{25}H_{32}F_2N_2O_2S+H^+$, 463.2225, found 463.2227.

(2*S*)-2-[(2-Chlorophenyl)methyl]-3-(2-fluorospiro[4,5-dihydrothieno[2,3-*c*]pyran-7,4'-piperidine]-1'-yl)-*N*-methyl-propanamide, ((*S*)-10b)—DIPEA (0.89 g, 6.85 mmol) was added to a solution of **8b** (0.48 g, 1.14 mmol) in CH_2Cl_2 (20 mL), followed by methanamine hydrochloride (0.23 g, 3.43 mmol), EDCI hydrochloride (0.44 g, 2.28 mmol) and HOBt (0.31 g, 2.28 mmol). The reaction mixture was stirred at r.t. overnight, diluted with CH_2Cl_2 (50 mL), washed with $NaHCO_3$ (aq.) and brine, dried over Na_2SO_4, and evaporated to dryness. The crude material was purified with TLC (CH_2Cl_2: MeOH; 25: 1 v/v) to afford **10c** as an off-white solid (0.37 g, 75% yield). Chiral HPLC of **10b** on a Daicel AD-H column (5 μm; 21.2 × 250 mm) eluted with A: B (90: 10 v/v) (A: 0.1% DEA in hexane; B: 0.1% DEA in EtOH) at 12 mL/min with eluate monitored for absorbance at 214 nm gave (***S***)-**10b** (100 mg, t_R = 5.63 min); m.p.: 161.1–165.4 °C; $[\alpha]_D$ = −23.2° (*c*. 6.67 MeOH); ^{1}H-NMR (300 MHz, $CDCl_3$): δ 7.36–7.32 (m, 1H), 7.30–7.23 (m, 1H), 7.21–7.11 (m, 2H), 6.12 (d, *J* = 1.5 Hz, 1H), 3.88 (t, *J* = 5.7 Hz, 2H), 3.26 (d, *J* = 5.7 Hz, 1H), 2.88–2.61 (m, 8H), 2.24 (t, *J* = 11.7 Hz, 1H), 2.04–1.94 (m, 2H), 1.82–1.66 (m, 3H); LC-MS (ESI): *m/z*: 437$(M+1)^+$, purity 100%, t_R = 4.38 min, method 2; HRMS (ESI): calc'd for $C_{22}H_{26}ClFN_2O_2S+H^+$, 437.1460, found 437.1464.

(2*R*)-2-[(2-Chlorophenyl)methyl]-3-(2-fluorospiro[4,5-dihydrothieno[2,3-*c*]pyran-7,4'-piperidine]-1'-yl)-*N*-methyl-propanamide, ((*R*)-10b)—The chiral HPLC of **10b**, described above also gave (***R***)-**10b** (120 mg, *t* = 7.93 min); m.p.: 165.6–167.8 °C; $[\alpha]_D$ = +24° (*c*. 10.0 MeOH); ^{1}HNMR and LC-MS as for (***S***)-**10b**: purity 100%, t_R = 4.38 min, method 2; HRMS (ESI): calc'd for $C_{22}H_{26}ClFN_2O_2S+H^+$, 437.1460, found, 437.1468.

(2*S*)-2-[(2-Fluorophenyl)methyl]-3-(2-fluorospiro[4,5-dihydrothieno[2,3-*c*]pyran-7,4'-piperidine]-1'-yl)-*N*-methyl-propanamide, ((*S*)-10c)—DIPEA (1.37 g, 10.6 mmol) was added to a solution of **8a** (0.54 g, 1.33 mmol) in CH_2Cl_2 (20 mL), followed by methanamine hydrochloride (0.27 g, 4.00 mmol), EDCI hydrochloride (0.51 g, 2.66 mmol) and HOBt (0.41 g, 2.68 mmol). The reaction mixture was stirred at r.t. overnight, diluted with CH_2Cl_2 (50 mL), washed with $NaHCO_3$ (aq.) and brine, dried over Na_2SO_4, and evaporated to dryness. The residue was purified with TLC (CH_2Cl_2: MeOH; 25: 1 v/v) to afford **10c** as an off-white solid (0.41 g, 73% yield). Chiral HPLC of **10c** on a Daicel AD-H column: (5 μm; 21.2 × 250 mm) eluted at 15 mL/min with A: B (90: 10 v/v) (A: 0.1% DEA/hexane, B: 0.1% DEA/alcohol) with eluate monitored for absorbance at 214 nm gave (***S***)-**10c** as a white solid (0.18 g, t_R = 10.47 min); m.p.: 99.5–101.8 °C; $[\alpha]_D$ = −7.0° (*c*. 10.0 MeOH); ^{1}H-NMR (300 MHz, $CDCl_3$) δ 7.54 (br, s, 1H), 7.26–7.14 (m, 2H), 7.08–6.95 (m, 2H), 6.11 (s, 1H), 3.86 (t, *J* = 5.4 Hz, 2H), 3.25–3.13 (m, 1H), 2.82–2.58 (m, 8H), 2.53 (t, *J* = 5.4 Hz, 3H), 2.47–2.09 (m, 2H), 1.99 (d, *J* = 14.4 Hz, 2H), 1.87–1.52 (m, 2H); LC-MS (ESI) *m/z*: 421 $(M+1)^+$, purity: 100%, t_R = 4.48 min, method 2; HRMS (ESI): calc'd for $C_{22}H_{26}F_2N\ O_2S+H^+$: 421.1756; found 421.1756.

(2*R*)-2-[(2-Fluorophenyl)methyl]-3-(2-fluorospiro[4,5-dihydrothieno[2,3-*c*]pyran-7,4'-piperidine]-1'-yl)-*N*-methyl-propanamide, ((*R*)-10c)—The chiral HPLC of **10c**, described above, also gave (***R***)-**10c**, as a white solid (0.17 g; t_R = 16.98 min); $[\alpha]_D$ = +7.5° (*c*. 10.0 MeOH); ^{1}H-NMR and LC-MS, as for (***S***)-**10c**; purity: 100%, t_R = 4,48 min, method 2; HRMS (ESI): calc'd for $C_{22}H_{26}F_2N\,O_2S+H^+$, 421.1756, found 421.1762.

In Vitro NOP Receptor Binding—Radioligand binding assays are commonly used to determine the affinity (K_i) of a compound for binding to a particular receptor or target protein. A filtration-based [^{3}H]nociceptin binding assay was developed, based on previous assay formats,[29] with minor modifications. Assay incubations were performed in deep-well 96-well plates with [^{3}H]nociceptin (final assay concentration 0.2 nM) and 5–10 μg of membrane protein (isolated from CHO cells expressing cloned human NOP receptors) in a final volume of 0.5 mL of HEPES buffer (20 mM; pH 7.4) containing, 5 mM $MgCl_2$, 1 mM EGTA, 100 mM NaCl, and 0.1% bovine serum albumin (BSA). Incubations were performed for 60 min at r.t., which had been found previously to be optimal and terminated by filtration through glass fiber filters (Wallac filtermat A; pretreated with 0.3% polyethyleneimine for 1 h) on a cell harvester (Tomtec Inc, Hamden, CT). The filters were washed thrice with 5 mL of ice-cold Tris·HCl buffer (50 mM, pH 7.4). Filtermats were then dried and imbedded with Meltilex scintillant A and the radioactivity counted in a Microbeta scintillation counter (Wallac). Specific binding was determined by displacement with 100 nM unlabeled nociceptin. Curves were plotted as the percent of specific binding and IC_{50} values were determined using a sigmoidal dose response curve with variable slope using GraphPad Prism (GraphPad Software; San Diego, CA). K_i values were calculated from the IC_{50} by the equation of Cheng and Prusoff,[30] where $K_i = IC_{50} \times (1 + (L/K_d))^{-1}$. L is free ligand concentration and K_d is the equlibrium dissociation constant of [^{3}H]nociceptin at cloned human NOP receptors expressed in CHO cells, and was separately determined from a receptor saturation study as 0.16 ± 0.02 nM (n = 4)

In Vitro Functional Blockade of NOP Receptor Agonist-Mediated G-protein Activation – [^{35}S]GTPγS Binding—Agonist-mediated stimulation of G-protein coupled receptors results in the activation of membrane associated Gαβγ-protein heterotrimer complexes, and represents the first step in the transduction of extracellular signals to the modification of intracellular pathways. The first step in activation of receptor-mediated activation of Gαβγ-proteins heterotrimer is the exchange of Gα subunit bound guanosine diphosphate (GDP) for guanosine triphosphate (GTP). The binding of GTP to the Gα subunit causes dissociation of the heterotrimer subunits, Gβ and Gγ, resulting in the modulation of several intracellular signaling cascades. Receptor-mediated G-protein activation can be measured using the non-hydrolyzable radiolabeled analog of GTP, [^{35}S]GTPγS. Thus, the NOP receptor antagonist affinity (K_b) of test ligands was measured in membranes expressing cloned human NOP receptors with a [^{35}S]GTPγS binding assay, according to previously described protocols with minor modifications.[31,32]

Assays were conducted in deep-well 96 well plates in a 200-μL volume with the following buffer composition: 100 mM NaCl, 20 mM HEPES, 5 mM $MgCl_2$, 1 mM EDTA, 0.1% BSA, 3μM GDP, 0.5 nM [^{35}S]GTPγS. NOP receptor membrane suspension was added at a concentration of 20 μg protein per well and > 90% receptor stimulation was achieved with 300 nM nociceptin. In this assay, nociceptin is a full agonist (99.8 ± 7.06% relative efficacy; n = 14) with an EC_{50} of 2.4 nM using a 4 parameter fit. Wheat germ agglutinin-coated SPA (scintillation proxity assay) beads (Amersham, Arlington Hts., IL) were added at 1 mg per well to detect membrane-bound [^{35}S]GTPγS. Plates were sealed and incubated for 2 h at r.t. and then placed at 4 °C overnight to allow the SPA beads to settle. Plates were then counted for radioactivity in a Microbeta instrument (Wallac). Specific [^{35}S]GTPγS binding was determined as the difference in cpm observed in the absence and presence of 10 μM

unlabeled GTPγS. Data were plotted as the percent of specific [^{35}S]GTPγS bound from which IC_{50} values were determined using a sigmoidal dose response curve with variable slope and GraphPad Prism software (GraphPad Software). Antagonist affinity (K_b) was estimated according to Delapp et al.[31] using a modification of the equation of Cheng and Prusoff[30] where $K_b = IC_{50} \times (1 + (L/EC))^{-1}$

Characterization of Test Ligands in Rat In Vivo—Doses of the ligands, **10a–c**, to be given to rats were selected to be low but still allow accurate measurement by ex vivo LC-MS/MS. Thus, each test ligand (1 mg) was dissolved in β-cyclodextrin solution (25%; 1 mL) and then diluted to a final ligand concentration of 6 μg/mL. Each of these solutions was administered intravenously to separate groups of three or four rats, with each injection given in a volume of 0.5 mL/kg via the lateral tail vein. Rats were sacrificed at 10, 20, 40, or 60 min after ligand injection. Samples of hypothalamic and striatal tissue were dissected out, weighed and placed in conical centrifuge tubes on ice. Four volumes (w/v) of acetonitrile containing 0.1% formic acid were added to each tube. These samples were then homogenized using an ultrasonic probe and centrifuged at 3.75 *g* for 16 min. Supernatant liquid (100 μL) was diluted by adding sterile water (100–900 μL) in HPLC injection vials for subsequent LC-MS/MS analysis.

Ligands were analyzed with a model 1200 HPLC apparatus (Agilent Technologies, Palo Alto, CA) linked to an API 4000 mass spectrometer (Applied Biosystems, Foster City, CA, USA). The liquid chromatography was performed on a C18 column (2.1 × 50 mm; Agilent; part # 971700-907) eluted with 0.1% formic acid in water-acetonitrile (40: 60 by vol. for (***S***)-**10a** and (***S***)-**10b**, and 30:70 by vol. for (***S***)-**10c**) at 0.25 mL/min (t_R = 1.7, 1.4 and 3.0 min for (***S***)-**10a–c**, respectively). The ligands were detected by monitoring the precursor to product ion transitions, namely, 463.8 to 240.0 for (***S***)-**10a**, 438.325 to 240 for (***S***)-**10b** and 421.154 to 239.8 for (***S***)-**10c**. Standards were prepared by adding known quantities of analyte to samples of brain tissue from non-treated rats and processed as described above. In order to normalize for amount of ligand injected and animal weight, the concentration of injected ligand found in brain region tissue, was transformed to %SUV (standardized uptake value), as follows: CHO cells, and was separately determined from a receptor saturation study as 0.16 ± 0.02 nM (n = 4)

In Vitro Functional Blockade of NOP Receptor Agonist-Mediated G-protein Activation – [^{35}S]GTPγS Binding—Agonist-mediated stimulation of G-protein coupled receptors results in the activation of membrane associated Gαβg-protein heterotrimer complexes, and represents the first step in the transduction of extracellular signals to the modification of intracellular pathways. The first step in activation of receptor-mediated activation of Gαβγ-proteins heterotrimer is the exchange of Gα subunit bound guanosine diphosphate (GDP) for guanosine triphosphate (GTP). The binding of GTP to the Gα subunit causes dissociation of the heterotrimer subunits, Gβ and Gγ, resulting in the modulation of several intracellular signaling cascades. Receptor-mediated G-protein activation can be measured using the non-hydrolyzable radiolabeled analog of GTP, [^{35}S]GTPγS. Thus, the NOP receptor antagonist affinity (K_b) of test ligands was measured in membranes expressing cloned human NOP receptors with a [^{35}S]GTPγS binding assay, according to previously described protocols with minor modifications.[31,32]

Assays were conducted in deep-well 96 well plates in a 200-μL volume with the following buffer composition: 100 mM NaCl, 20 mM HEPES, 5 mM $MgCl_2$, 1 mM EDTA, 0.1% BSA, 3 μM GDP, 0.5 nM [^{35}S]GTPγS. NOP receptor membrane suspension was added at a concentration of 20 μg protein per well and > 90% receptor stimulation was achieved with 300 nM nociceptin. In this assay, nociceptin is a full agonist (99.8 ± 7.06% relative efficacy; n = 14) with an EC_{50} of 2.4 nM using a 4 parameter fit. Wheat germ agglutinin-coated SPA

(scintillation proxity assay) beads (Amersham, Arlington Hts., IL) were added at 1 mg per well to detect membrane-bound [^{35}S]GTPγS. Plates were sealed and incubated for 2 h at r.t. and then placed at 4 °C overnight to allow the SPA beads to settle. Plates were then counted for radioactivity in a Microbeta instrument (Wallac). Specific [^{35}S]GTPγS binding was determined as the difference in cpm observed in the absence and presence of 10 μM unlabeled GTPγS. Data were plotted as the percent of specific mixture was then heated at 80 °C for 5 min, after which the crude reaction mixture was diluted with water (500 μL). The product was injected onto a Luna C18 column (10 μm, 10 × 250 mm; Phenomenex) eluted with MeCN (A)-0.1M-$HCOONH_4$ (B) (70: 30 v/v) at 6.5 mL/min for [^{11}C](***S***)-**10a**, with A: B (60: 40 v/v) at 6.5 mL/min for [^{11}C](***S***)-**10b**, and with A: B (50: 50 v/v) at 8.5 mL/min for 5 min, and then 6 mL/min, for [^{11}C](***S***)-**10c** or [11C](***R***)-**10c**. Eluate was monitored for absorbance at 235 nm (Beckman 166 UV detector) and for γ-radiation with a semiconductor pin-diode detector (Bioscan). The radioligand peak (t_R = 11.20, 10.1, 11.83 and 11.83 min for [[^{11}C](***S***)-**10a–c** and [^{11}C](***R***)-**10c**, respectively) was collected and mobile phase removed under high vacuum at 80 °C for 1 min. Ethanol (1.5 mL) was added to dissolve the radioactive residue and the solution then diluted with saline (13.5 mL). Finally, this solution was sterilized by filtration through a sterile Millex-MP filter (Millipore Corp.) to provide radioligand ready for intravenous injection, pending HPLC analysis.

Each radioligand was analyzed for radiochemical purity, specific activity and chemical purity with reverse phase HPLC (see Supporting Information for elution conditions and retention times). Eluates were monitored for radioactivity (pin diode detector; Bioscan) and absorbance at 235 nm. The response of the absorbance detector was calibrated for mass of radioligand to allow determination of the mass of carrier in radioligand injectate for subsequent calculation of specific radioactivity (as Ci of radioligand/μmol of carrier). Samples were injected alone for the radiochemical purity, chemical purity and specific activity measurements, and then co-injected with the reference non-radioactive compound to check for co-elution and thus radiotracer identity. The identity of each product was verified by LC-MS/MS of carrier in the radioligand preparation on a Finnigan LCQ DECA instrument.

The chiral purity of [^{11}C](***S***)-**10c** was confirmed by HPLC on a Chiralpak AD column (4.6 × 250 mm) eluted at 2.0 mL/min with mobile phase composed of 0.1% TEA in hexane-0.1% TEA in isopropyl alcohol (96: 4 v/v). [^{11}C](***S***)-**10c** and (***S***)-**10c** had retention times of 10.7 min, and the enantiomer (***R***)-**10c** a retention time of 12.35 min (see Supporting Information).

Computation and Measurement of Lipophilicity—The *cLogD* values for ligands (***S***)-**10a–c** at pH 7.4 were computed with Pallas 3.7 software (CompuDrug). The *LogD* value of (***S***)-**10c** (at pH 7.4) was measured with [^{11}C](***S***)-**10c** by a previously described method.[35,36] *LogD* values at pH 7.4 were also measured for enantiomers of ligands **10a–c** by a shake flask method.

PET Experiments in Monkeys—For each scanning session, the subject monkey was immobilized with ketamine and maintained under anesthesia with 1–3% isoflurane in oxygen. An intravenous perfusion line, filled with saline (0.9% w/v), was used for bolus injection of high purity radioligand (> 99.9% radiochemical purity). PET serial dynamic images of brain were obtained for up to 90 min on either an Advance (GE Medical Systems, WI) or Focus 220 (Siemens) PET camera.

Decay-corrected time-activity curves (TACs) were obtained for 16 irregular volumes of interest (VOIs) in brain (anterior cingulate, amygdala, basal frontal cortex, caudate, cerebellum hippocampus, hypothalamus, insula, lateral temporal cortex, medial temporal cortex, occipital cortex, parietal cortex, posterior cingulate, prefrontal cortex, putamen, and

thalamus). Radioactivity levels in VOIs were normalized for injected dose and monkey weight by expression as a % standardized uptake value (%SUV):

$$\%\text{SUV} = [(\%\text{injected dose per mL}) \times \text{body weight in g}]$$

The following scans were performed with [^{11}C](***S***)-**10c**. *Baseline scans*: Five male monkeys (9.5–12.9 kg) received brain scans at baseline after a bolus intravenous injection of radioligand (4.92–6.60 mCi; dose of carrier (***S***)-**10c**, 0.127–0.355 nmol/kg), which was given at 10 min following intravenous injection of vehicle for pre-blocking agent. *Pre-block scans*: These were performed on the same day at about 3 h after the baseline scan in each of the five monkeys. In each case, the NOP pre-block agent **1** (1 mg/kg, i.v) was administered over 2 min at 10 min before radioligand (4.92–6.70 mCi; dose of carrier, 0.190–0.337 nmol/kg). *Displacement scans*: One monkey (11.47 kg) was scanned with [^{11}C](***S***)-**10c** (6.20 mCi; dose of carrier (***S***)-**10c**, 0.457 nmol/kg) with displacer **1** (1 mg/kg, i.v.) administered over 2 min at 40 min from the start of the scan. One monkey (7.2 kg) was scanned with [^{11}C](***S***)-**10c** (6.78 mCi; dose of carrier (***S***)-**10c**, 0.794 nmol/kg) with naloxone (5 mg/kg, i.v.) administered over 2 min at 37 min from the start of the scan. Baseline and pre-block scans were also performed with [^{11}C](***R***)-**10c** in one monkey (wt., 9.9 kg; dose, 6.53 and 6.72 mCi; carrier, 0.496 and 0.366 nmol/kg), [^{11}C](***S***)-**10a** in two monkeys (wt., 11.5 and 12 kg; doses, 4.78–5.93 mCi; carrier, 0.0912–0.329 nmol/kg) and [^{11}C](***S***)-**10b** in three monkeys (wt., 9.1–10.1 kg; doses, 5.33–5.92 mCi; carrier, 0.123–0.411 nmol/kg). A total of 6 monkeys were used for all PET experiments, with one monkey studied with each of the three radioligands (***S***)-**10a–c** under baseline and preblock conditions to provide a within-subject comparison.

Stability of [^{11}C](*S*)-10c in Monkey Whole Blood and Plasma in Vitro, and in Buffer—[^{11}C](***S***)-**10c** was incubated for 30 min in whole monkey blood (0.5 mL). A blood sample (0.20 mL) was removed and added to water (0.3 mL) to lyse the cells. A sample (0.45 mL) was then removed added to acetonitrile (0.7 mL), and centrifuged. Then the supernatant liquid was analyzed by reverse phase radio-HPLC on a Novapak C18 column (4 μm; 100 × 800 mm; Waters Corp.) housed in a radial compression module (RCM 100) and eluted with MeOH: H_2O: Et_3N (80: 20: 0.1 by vol.) at 2.5 mL/min. The stability of [^{11}C](***S***)-**10c** to incubation in sodium phosphate buffer (0.15 M, pH 7.4) for 2.5 h at r.t. was also assessed by reverse phase HPLC.

Plasma Protein Binding of [^{11}C](*S*)-10c[37]—The radioligand was added to human plasma, pooled from two subjects, and placed at the top of an "Amicon" Centrifree filter unit (200 μL/unit) and filtered by ultra centrifugation at 5000 × *g*. Then the filtrate (50 μL), remainder of filtrate and all components of the filter units were counted for radioactivity to allow calculation of f_P. The procedure was also perfomed with plasma pooled from 2 monkeys. Each measurement was made thrice. Values do not take account of non-specific binding to the filter housing.

Emergence of Radiometabolites of [^{11}C](*S*)-10c in Monkey Plasma In Vivo— During each of six PET scans (three baseline and three preblock) with [^{11}C](***S***)-**10c**, blood samples were drawn periodically from the monkey femoral artery and collected in heparin-treated Vacutainer tubes. The samples were centrifuged and the plasma separated. A sample of plasma (0.45 mL) was mixed with acetonitrile (0.7 mL) and centrifuged. The supernatant liquid was analyzed with radio-HPLC on a Novapak C18 column (4 μm; 8 × 100 mm) eluted at 2.5 mL/min with MeOH/H_2O/Et_2N (80: 20: 0.1 by vol.). The time-courses for percentages of radioactivity in plasma represented by [^{11}C](***S***)-**10c** and its radiometabolites were calculated.[38]

[$^3H_3$](*S*)-10c Autoradiography—Male littermates of NOP knockout and 129/S6 wild-type mice were generated by heterozygous matings (kindly provided by Dr. John Pintar, UMDNJ, Piscataway, NJ). Animals were euthanized by decapitation, and the brains were removed and frozen on dry-ice. Twelve-μm frozen coronal sections from both genotypes were thaw-mounted onto chrome alum/gelatin coated slides and stored at −70 °C until used. Sections were pre-incubated at 25 °C for 15 min in Tris-HCl buffer (50 mM) containing, 5 mM $MgCl_2$ (Mallinckrodt), 1 mM EDTA (EM Science), and 0.1% BSA. Incubations were conducted in the same buffer containing 0.6 nM [$^3H_3$](***S***)-**10c** at 25°C for 120 min. Non-specific binding was determined on adjacent sections in the presence of the NOP receptor antagonist **1** at a concentration of 10 μM. Sections were washed twice on ice for 10 min in pre-incubation buffer containing no BSA, followed by a rinse in ice-cold distilled water. Slides were dried under a cool stream of air and opposed to a phosphorimaging plate (BAS-IP TR 2025, Fuji, Tokyo, Japan) for 4 days. The plate was scanned using a BAS-5000 imager (Fuji). Quantification was performed with MCID 7.0 imaging software (Interfocus Imaging, UK). ^{3}H-Microscales (Amersham) were exposed with the slides and used for quantification of binding.

Supplementary Material

Refer to Web version on PubMed Central for supplementary material.

Acknowledgments

This study was supported by the Intramural Research Program of the National Institutes of Health (NIH), specifically the National Institute of Mental Health (NIMH). We thank the NIH PET Department for radioisotope production, Dr. Talakad G. Lohith, Dr. Harushige Ozaki, Ms. Leah Dickstein and Mr. Robert L. Gladding for assistance with PET imaging, Dr. Fabrice G. Siméon and Ms. Cheryl L. Morse for contribution to radiochemistry, and Dr. H. Umesha Shetty for LC-MS measurements.

Abbreviations

AUC	area-under-the-curve
Boc	*t*-butyloxycarbonyl
BSA	bovine serum albumin
DEA	diethylamine
DIPEA	di-isopropylethylamine
DMEA	dimethylethylamine
DMSO	dimethyl sulfoxide
EDCI	1-ethyl-3(dimethylaminopropyl)-carbodiimide
f_P	plasma free fraction
GDP	guanosine diphosphate
GTP	guanosine triphosphate
HOBt	1-hydroxybenzotriazole
MRI	magnetic resonance imaging
NCA	no-carrier-added
NFSI	*N*-fluoro-*N*-(phenylsulfonyl)benzenesulfonamide
NOP	nociceptin/orphanin FQ peptide

PET	positron emission tomography
r.t.	room temperature
SPA	scintillation proxity assay
SUV	standardized uptake value
TAC	time-activity curve
TEA	triethylamine
THF	tetrahydrofuran
TFA	trifluoracetic acid
VOI	volume of interest

References

[1]. Meunier JC, Mollereau C, Toll L, Suaudeau C, Moisand C, Alvinerie P, Butour JL, Guillemot JC, Ferrara P, Monsarrat B, Mazarguil H, Vassart G, Parmentier M, Costentin J. Isolation and structure of the endogenous agonist of opioid-like ORL 1 receptor. Nature. 1995; 377:532–535. [PubMed: 7566152]

[2]. Reinschied RK, Nothacker H-P, Bourson A, Ardati A, Henningsen RA, Bunzow JR, Grandy DK, Langen H, Monsma F Jr. Civelli O. Orphanin FQ: a neuropeptide that activates an opioid-like G-protein coupled receptor. Science. 1995; 270:792–794. [PubMed: 7481766]

[3]. Mogli JS, Pasternak GW. The molecular and behavioral pharmacology of the orphanin FQ/nociceptin peptide and receptor family. Pharmacol. Rev. 2001; 53:381–415. [PubMed: 11546835]

[4]. Lambert DG. The nociceptin/orphanin FQ receptor: a target with broad therapeutic potential. Nature Rev. Drug Discovery. 2008; 7:694–710.

[5]. Murphy NP. The nociceptin/orphamin FQ system as a target for treating alcoholism. CNS & Neurological Disorders - Drug Targets. 2010; 9:87–93. [PubMed: 20201819]

[6]. Phelps ME. Positron emission tomography provides molecular imaging of biological processes. Proc. Natl. Acd. Sci., USA. 2000; 97:9226–9233.

[7]. Wong DF, Gründer G, Brašić JR. Brain imaging research: does the science serve clinical practice? Int. Rev. Psychiatry. 2007; 19:541–558. [PubMed: 17896234]

[8]. Gibson RE, Burns HD, Hamill TG, Eng WS, Francis BE, Ryan C. Non-invasive radiotracer imaging as a tool for drug development. Curr. Radiopharm. Design. 2000; 6:973–989.

[9]. Lee CM, Farde L. Using positron emission tomography to facilitate CNS drug development. TIPs. 2006; 27:310–316. [PubMed: 16678917]

[10]. Pike VW. Positron-emitting radioligands for studies in vivo — probes for human psychopharmacology. J. Psychopharmacology. 1993; 7:139–158.

[11]. Laruelle M, Slifstein M, Huang Y. Relationships between radiotracer properties and image quality in molecular imaging of the brain with positron emission tomography. Mol. Imaging Biol. 2003; 5:363–375. [PubMed: 14667491]

[12]. Patel S, Gibson R. In vivo site-directed radiotracers: a mini-review. Nucl. Med. Biol. 2008; 35:805–815. [PubMed: 19026942]

[13]. Pike VW. PET Radiotracers: crossing the blood-brain barrier and surviving metabolism. TIPs. 2009; 30:431–440. [PubMed: 19616318]

[14]. Neal CR Jr. Mansour A, Reinscheid R, Nothacker HP, Civelli O, Akil H, Watson SJ Jr. Opioid receptor-like (ORL1) receptor distribution in the rat central nervous system: comparison of ORL receptor mRNA expression with 125I-(^{14}Tyr)-orphanin FQ binding. J. Comp. Neurol. 1999; 412:563–605. [PubMed: 10464356]

[15]. Florin S, Meunier JC, Costentin J. Autoradiographic localization of [^{3}H]nociceptin binding sites in the rat brain. Brain Res. 2000; 880:11–16. [PubMed: 11032985]

[16]. Letchworth SR, Mathis JP, Rossi GC, Bodnar RJ, Pasternak GW. Autoradiographic localization of 125I[Tyr^{14}]orphanin FG/nociceptin and 125I[Tyr^{10}]orphanin FQ/nociceptin(1–11) binding sites in rat brain. J. Comp. Neurol. 2000; 423:319–329. [PubMed: 10867661]

[17]. Bojnik E, Farkas J, Magyar A, Tömböly C, Güçlü U, Gündüz O, Borsodi A, Corbani M, Benyhe S. Selective and high affinity labeling of neuronal and recombinant nociceptin receptors with the hexapeptide radioprobe [^{3}H]Ac-RYYRIK-ol. Neurochem. Int. 2009; 55:458–466. [PubMed: 19414055]

[18]. Bridge KE, Wainwright A, Reilly K, Oliver KR. Autoradiographic localization of 125I[Tyr14] nocicepetin/orphanin FQ binding sites in macaque primate CNS. Neurosci. 2003; 118:513–523.

[19]. Largent-Milnes TM, Vanderah TW. Recently patented and promising ORL-1 ligands: where have we been and where are we going? Expert Opinion Therapeutic Patents. 2010; 20:291–305.

[20]. Spagnola B, Carra G, Fantin M, Fischetti C, Hebbes C, McDonald J, Barnes TA, Rizzi A, Trapella C, Fanton G, Morari M, Lambert DG, Regoli D, Calo G. Pharmacological characterization of the nociceptin/orphanin FQ receptor antagonist SB-612111 [(−)-*cis*-1-methyl-7-[[4-(2,6-dichlorophenyl)piperidin-1-yl]methyl]-6,7,8,9-tetrahydro-5*H*-benzocyclohepten-5-ol]: in vitro studies. J. Pharmacol. Exp. Ther. 2007; 321:961–967. [PubMed: 17329552]

[21]. Rizzi A, Gavioli EC, Marzola G, Spagnola B, Zucchini S, Ciccocioppo R, Trapella C, Regoli D, Calo G. Pharmacological characterization of the nociceptin/orphanin FQ receptor antagonist SB-612111 [(−)-*cis*-1-methyl-7-[[4-(2,6-dichlorophenyl)piperidin-1-yl]methyl]-6,7,8,9-tetrahydro-5*H*-benzocyclohepten-5-ol]: in vivo studies. J. Pharmacol. Exp. Ther. 2007; 321:968–974. [PubMed: 17329551]

[22]. Chernet E, Martin LJ, Li D, Need AB, Barth VN, Rash KS, Phebus LA. Use of LC/MS to assess brain tracer distribution in preclinical in vivo receptor occupancy studies: Dopamine D2, serotonin 2A and NK-1 receptors as examples. Life Sci. 2005; 78:340–346. [PubMed: 16139310]

[23]. Barth VN, Chernet E, Martin LJ, Rash KS, Morin M, Phebus LA. Comparison of rat dopamine D2 receptor occupancy for a series of antipsychotic drugs measured using radiolabeled or nonlabeled raclopride tracer. Life Sci. 2006; 78:3007–3012. [PubMed: 16434058]

[24]. Waterhouse RN. Determination of lipophilicity and its use as a predictor of blood-brain barrier penetration of molecular imaging agents. Mol. Imaging Biol. 2003; 5:376–389. [PubMed: 14667492]

[25]. Jones AKP, Luthra SK, Mazière, B., Pike VW, Loc'h C, Crouzel C, Syrota A, Jones T. Regional cerebral opioid receoptros studies with [^{11}C]diprenorphine in normal volunteers. J. Neurosci. Methods. 1988; 23:121–129. [PubMed: 2833666]

[26]. Galynker I, Schlyer DJ, Dewey SL, Fowler JS, Logan J, Gatley SJ, MacGregor RR, Ferrieri RA, Holland MJ, Brodie J, Simom E, Wolf AP. Opioid receptor imaging and displacement studies with [6-*O*-[^{11}C]methyl]buprenorphine in baboon brain. Nucl. Med. Biol. 1996; 23:325–331. [PubMed: 8782244]

[27]. Zoghbi SS, Anderson KB, Jenko KJ, Innis RB, Pike VW. On the quantitative relationship between radiotracer lipophilicity and plasma free fraction. NeuroImage. 2010; 52(Suppl. 1):S221.

[28]. Clark, JD.; Baldwin, RL.; Bayne, KA.; Brown, MJ.; Gebhart, GF.; Gonder, JC.; Gwathmey, JK.; Keeling, ME.; Kohn, DF.; Robb, JW.; Smith, OA.; Steggerda, J-AD.; VandeBer, JL. Guide for the Care and Use of Laboratory Animals. National Academy Press; Washington DC: 1996.

[29]. Ardati A, Henningsen RA, Higelin J, Reinscheid RK, Civelli O, Monsma FJ Jr. Interaction of [^{3}H]orphanin FQ and 125I-Tyr14-orphanin FQ with the orphanin FQ receptor: kinetics and modulation by cations and guanine nucleotides. Mol. Pharmacol. 1997; 51:816–824. [PubMed: 9145920]

[30]. Cheng Y, Prusoff WH. Relationship between the inhibition constant (K_I) and the concentration of inhibitor which causes 50 percent inhibition (I_{50}) of an enzymatic reaction. Biochem. Pharmacol. 1973; 22:3099–3108. [PubMed: 4202581]

[31]. Delapp NW, McKinzie JH, Sawyer BD, Vandergriff A, Falcone J, McClure D, Felder CC. Determination of [^{35}S]guanosine-5'-*O*-(3-thio)triphosphate binding mediated by cholinergic muscarinic receptors in membranes from Chinese hamster ovary cells and rat striatum using an anti-G protein scintillation proximity assay. J. Pharmacol. Exp. Ther. 1999; 289:946–955. [PubMed: 10215674]

[32]. Ozaki S, Kawamoto H, Itoh Y, Miyaji M, Azuma T, Ichikawa D, Nambu H, Iguchi T, Iwasawa Y, Ohta H. In vitro and in vivo pharmacological characterization of J-113397, a potent and selective non-peptidyl ORL1 receptor antagonist. Eur. J. Pharmacol. 2000; 402:45–53. [PubMed: 10940356]

[33]. Christman DR, Finn RD, Karlström K, Wolf AP. The production of ultra high specific activity ^{11}C-labeled hydrogen cyanide, carbon dioxide, carbon monoxide and methane via the ^{14}N(p,α)^{11}C reaction. Int. J. Appl. Radiat. Isot. 1975; 26:435–442.

[34]. Larsen P, Ulin J, Dahlström K, Jensen M. Synthesis of [^{11}C]iodomethane by iodination of [^{11}C]methane. Appl. Radiat. Isot. 1997; 48:153–157.

[35]. Zoghbi SS, Baldwin RM, Seibyl JP, Charney DS, Innis RB. A radiotracer technique for determining apparent pKa of receptor-binding ligands. J. Label. Compd. Radiopharm. 1997; 41:136.

[36]. Briard E, Zoghbi SS, Imaizumi M, Gourley JP, Hong J, Cropley V, Fujita M, Innis RB, Pike VW. Synthesis and evaluation of two sensitive ^{11}C-labeled aryloxyanilide ligands for imaging brain peripheral benzodiazepine receptors in vivo. J. Med. Chem. 2008; 51:17–30. [PubMed: 18067245]

[37]. Gandelman MS, Baldwin RM, Zoghbi SS, Zea-Ponce Y, Innis RB. Evaluation of ultrafiltration for the free-fraction determination of single photon emission computed tomography (SPECT) radiotracers: β-CIT, IBF, and iomazenil. J. Pharm. Sci. 1994; 83:1014–1019. [PubMed: 7965658]

[38]. Zoghbi SS, Shetty UH, Ichise M, Fujita M, Imaizumi M, Liow JS, Shah J, Musachio JL, Pike VW, Innis RB. PET imaging of the dopamine transporter with [^{18}F]FECNT: a polar radiometabolite confounds brain radioligand measurements. J. Nucl. Med. 2006; 47:520–527. [PubMed: 16513622]

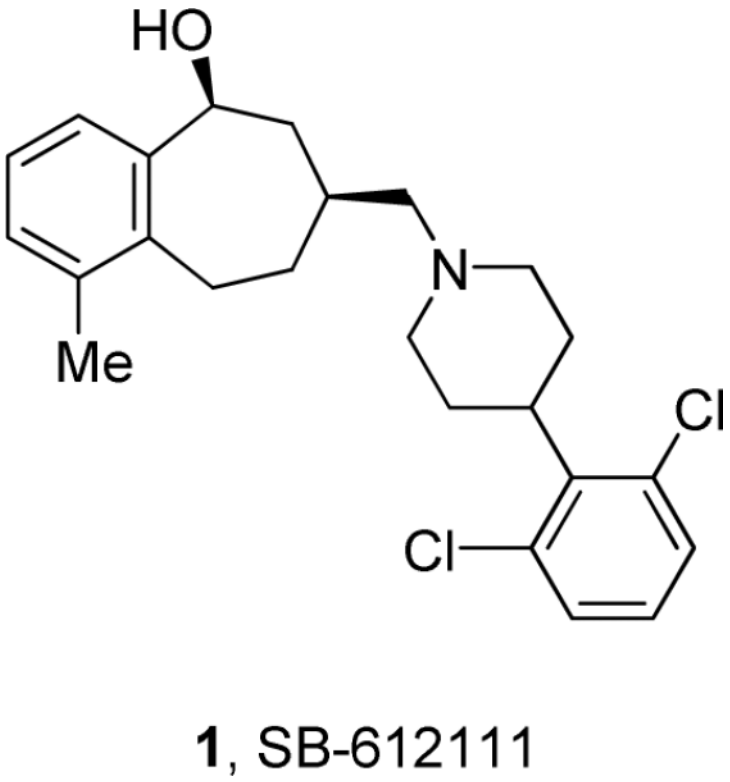

1, SB-612111

Chart 1.
Structure of **1**.

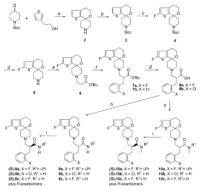

Scheme 1.

Synthesis of NOP ligands, **9a–c** and **10a–c**, and their enantiomers.

Reagents and conditions: (a) 1) TFA/CH_2Cl_2, r.t.; 2) 10% NaOH aq.; (b) di-*t*-butyl dicarbonate, TEA, CH_2Cl_2; (c) *n*-BuLi, −78 °C, NFSI, THF; (d) 4M HCl in dioxane, CH_2Cl_2, r.t.; (e) *t*-butyl acrylate, TEA,THF, reflux; (f) 1) $LiN(TMS)_2$, 1M THF, 1,3-dimethyl-tetrahydropyrimidin-2(1*H*)-one, THF, −78 °C, 2) 2-F-benzyl bromide or 2-Cl-benzyl bromide; (g) TFA/CH_2Cl_2, r.t.; (h) EDCI, HOBt, DIPEA, CH_2Cl_2, NH_4Cl or appropriate amine; (i) chiral HPLC separation.

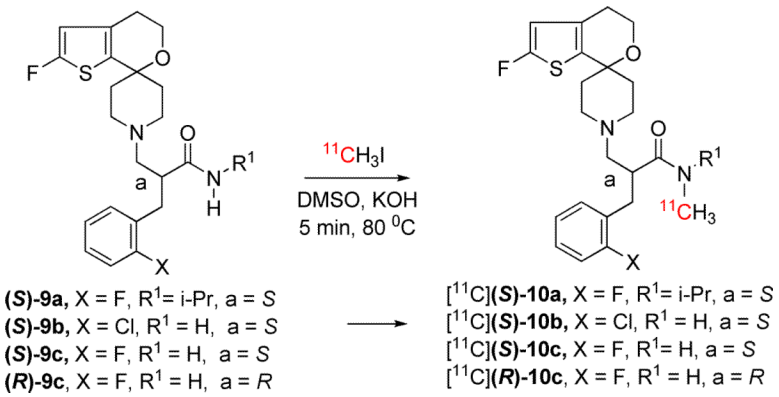

Scheme 2.
Radiolabeling of NOP ligands.

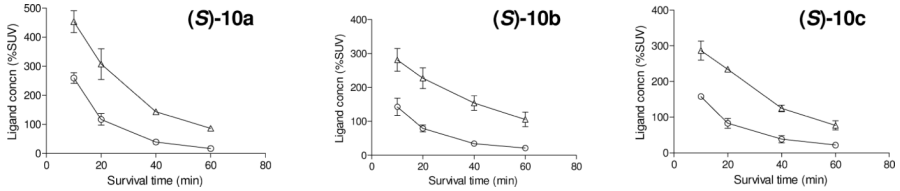

Figure 1.

Time-courses of normalized ligand concentrations (%SUV) in rat hypothalamus (Δ) and striatum (◯) after i.v. injection of non-radioactive NOP ligand (***S***)-**10a**, (***S***)-**10b** or (***S***)-**10c**(3 μg/kg, i.v.), measured ex vivo with LC-MS/MS. Error bars are S.D. (where not visible they are within the symbol size).

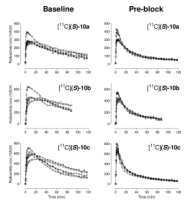

Figure 2.

Brain region time-activity curves in monkey after injection of radioligands [^{11}C](***S***)-**10a–c** in baseline and in pre-block experiments, in which NOP preblocker **1** (2 mg/kg, i.v.) was given at 10 min before radioligand. For each radioligand, the baseline and pre-block experiments were conducted about 3 h apart in the same monkey. Key: hypothalamus (◯), cerebellum (◇), caudate (▽), amygdala (Δ), lateral temporal cortex (□). Time-activity curves for other examined regions as listed in the experimental were generally similar to the non-cerebellar curves.

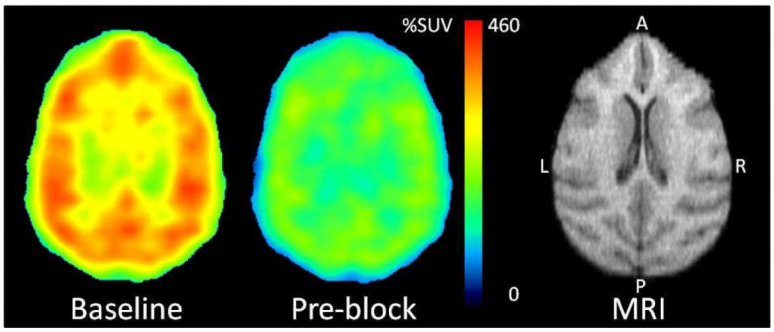

Figure 3.

Horizontal PET images of monkey brain at the level of the caudate acquired between 0 and 100 min after intravenous injection of [^{11}C](***S***)-**10c** under baseline and pre-block conditions. The corresponding magnetic resonance imaging (MRI) scan shows PET scan orientation and anatomy.

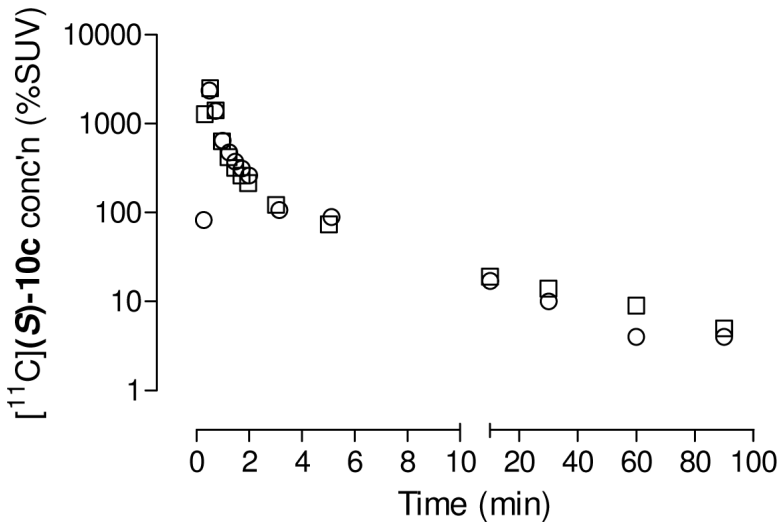

Figure 4.
Time-course of concentration of umetabolized [^{11}C](***S***)-**10c** in plasma after intravenous injection into monkey under baseline (◯) and pre-blocked conditions (□).

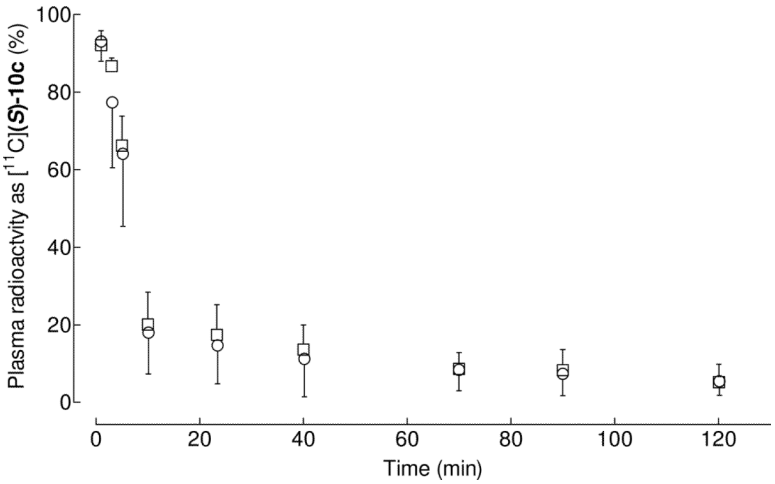

Figure 5.

Percentage of radioactivity in plasma represented by [^{11}C](***S***)-**10c** during PET scanning of three monkeys under baseline (◯) and pre-block conditions (□). Error bars are S.D. values.

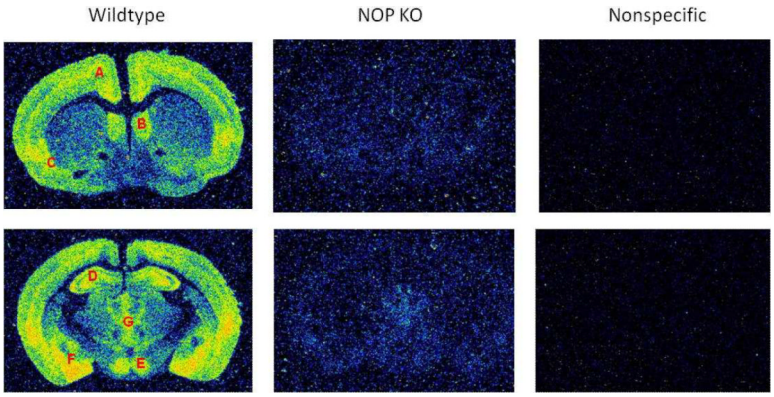

Figure 6.

Autoradiographs of binding of [$^3H_3$](***S***)-**10c** (0.6 nM) to 12-μm coronal sections of wild-type 129/S6 and NOP knockout mouse brain. Non-specific binding was determined in the presence of 10 μM **1** (from an adjacent section from wild-type mice). Wild-type 129/S6 mice exhibited high binding in numerous cortical regions (A), medial septum (B), dorsal endopiriform nucleus (C) hippocampus (D), vetromedial hypothalamic nuclues (E), amygdala (F), and central thalamus (G). No appreciable specific binding was observed in equivalent sections of NOP knockout mouse brain.

Table 1

Receptor binding affinities, antagonist activities, and lipophilicities of NOP ligands.

Ligand	[a]NOP Receptor binding K_i (nM)	[a]NOP Antagonist activity K_b (nM)	cLogD[b]
1	0.253 ± 0.151	0.258 ± 0.129	4.98
(*S*)-9a	0.231 ± 0.050	0.228 ± 0.050	4.08
(*R*)-9a	4.51 ± 1.05	5.64 ± 1.05	4.08
(*S*)-9b	0.101 ± 0.029	0.110 ± 0.021	3.41
(*R*)-9b	17.1 ± 2.54	7.36 ± 0.019	3.41
(*S*)-9c	0.106 ± 0.049	0.173 ± 0.084	2.95
(*R*)-9c	5.61 ± 2.74	8.65 ± 5.19	2.95
(*S*)-10a	0.137 ± 0.048	0.141 ± 0.032	4.39
(*R*)-10a	10.2 ± 2.85	15.8 ± 3.48	4.39, (4.47)[c]
(*S*)-10b	0.090 ± 0.016	0.099 ± 0.048	3.68
(*R*)-10b	9.08 ± 1.04	5.79 ± 1.05	3.68, (3.90)[c]
(*S*)-10c	0.150 ± 0.062	0.069 ± 0.015*	3.27, (3.50)[c], (3.41 ± 0.07, n = 6)[d]
(*R*)-10c	5.32 ± 1.03	7.92 ± 1.05	3.27

[a]Assays were performed in triplicate except for that with an asterisk (n = 2). Data are mean ± S.E. [^{3}H]Nociceptin was used as reference NOP radioligand in a binding assay using human recombinant NOP receptors expressed in CHO cells. Antagonist activity was determined in an assay of receptor-mediated G-protein activation using [^{35}S]GTPγS and membranes expressing cloned human NOP receptors. See methods for assay details.

[b]Computed with Pallas software. Values in parentheses are measured values.

[c]*LogD* measured with non-radioactive compound and shake-flask method.

[d]*LogD* value (mean ± SD) measured with [^{11}C]**(*S*)-10c**.

Table 2

NOP Receptor-specific to non-specific binding ratios for radioligands [^{11}C]**(*S*)-10a-c**, in monkey estimated from a) brain-averaged AUCs over 0–90 min (Method A), or b) over 30–90 min (Method B).

Ligand	Specific to non-specific ratio[a]		
	n	Method A	Method B
[^{11}C]**(*S*)-10a**	2	0.19, 0.44	0.53, 0.84
[^{11}C]**(*S*)-10b**	3	0.66 ± 0.26	1.31 ± 0.35
[^{11}C]**(*S*)-10c**	5	0.62 ± 0.36	1.28 ± 0.70

[a]The NOP receptor-specific to non-specific binding ratio was calculated as [($AUC_{baseline}/AUC_{preblock}$)–1], where the AUCs are measured over the same time interval.